Haldane-gap excitations in the low-H_c one-dimensional quantum antiferromagnet $Ni(C_5D_{14}N_2)_2N_3(PF_6)$

A. Zheludev,[1] Y. Chen,[2] C. L. Broholm,[2,3] Z. Honda,[4] and K. Katsumata[4]
[1]*Physics Department, Brookhaven National Laboratory, Upton, New York 11973-5000*
[2]*Department of Physics and Astronomy, Johns Hopkins University, Baltimore, Maryland 21218*
[3]*NIST Center for Neutron Research, National Institute of Standards and Technology, Gaithersburg, Maryland 20899*
[4]*RIKEN (The Institute of Physical and Chemical Research), Wako, Saitama 351-0198, Japan*
(Received 13 March 2000; revised manuscript received 21 July 2000; published 15 February 2001)

Inelastic neutron scattering on deuterated single-crystal samples is used to study Haldane-gap excitations in the new $S=1$ one-dimensional quantum antiferromagnet $Ni(C_5D_{14}N_2)_2N_3(PF_6)$, that was recently recognized as an ideal model system for high-field studies. The Haldane gap energies $\Delta_x=0.42(3)$ meV, $\Delta_y=0.52(6)$ meV, and $\Delta_z=1.9(1)$ meV, for excitations polarized along the *a*, *b*, and *c* crystallographic axes, respectively, are measured. The dispersion relation is studied for momentum transfers both along and perpendicular to the chains' direction. The in-chain exchange constant $J=2.8$ meV is found to be much larger than interchain coupling, $J_y=1.8(4)\times10^{-3}$ meV and $J_x=4(3)\times10^{-4}$ meV, along the *b* and *a* axes, respectively. The results are discussed in the context of future experiments in high magnetic fields.

DOI: 10.1103/PhysRevB.63.104410 PACS number(s): 75.40.Gb, 75.50.Ee, 75.10.Jm, 73.30.+y

I. INTRODUCTION

The unique properties of the one-dimensional (1D) integer-spin Heisenberg antiferromagnet (HAF) have captivated the minds of condensed matter physicists for the last 20 yr. In total defiance of the quasiclassical picture of magnetism, the ground state in this system is a spin-singlet: a ''quantum spin liquid'' with only short-range (exponentially decaying) spin correlations. The excitation spectrum is also unique and, even in the absense of any magnetic anisotropy, features a so-called Haldane energy gap.[1] The wealth of theoretical and experimental results accumulated to date provides a fairly complete understanding of the physics involved, and few mysteries remain as far as the behavior of the idealized model is concerned. Particularly revealing was the neutron scattering work done on real quasi-one-dimensional (1D) $S=1$ HAF compounds such as $CsNiCl_3$,[2] $Ni(C_2H_8N_2)_2NO_2(ClO_4)$(NENP),[3] and Y_2BaNiO_5.[4]

One of the few remaining unresolved issues is the behavior of Haldane-gap antiferromagnets in high magnetic fields. An external magnetic field splits the triplet of Haldane excitations,[5,3,6–9] driving one of the modes to zero energy at some critical field H_c. At this soft-mode quantum phase transition, long-range antiferromagnetic correlations appear. In essence, the external field suppresses zero-point quantum spin fluctuations that are responsible for the finite equal-time spin correlation length. Despite the success of high-field bulk studies of several materials, it has been highly frustrating that for most systems the high values of the critical fields preclude neutron scattering experiments. As a result, the properties of the high-field phase are still largely unknown. It is even unclear whether or not the high-field phase is commensurate, and virtually nothing is known about the excitation spectrum.

Traditionally, NENP was the workhorse of high-field studies. For this compound large single crystal samples can be fabricated, and the critical field $H_c=9$ T (when applied parallel to the chain axis) is, in principle, accessible in a neutron-scattering experiment. In practice, however it is easier to perform measurements with a magnetic field applied perpendicular to the spin chains. The corresponding critical field for NENP is, unfortunately, much larger: $H_c\approx11$–13 T. In any case, measurements deep within the high-field phase are not possible. Moreover, due to certain structural features, there is a crossover rather than a true phase transition to high field phase in NENP. This is because the *g* tensors of the $S=1$ Ni^{2+} ions are staggered in this compound and lead to an effective staggered field when an external uniform field is applied.[10–12] As a result, staggered magnetization appears at arbitrary weak applied fields, and there is no additional symmetry breaking that occurs at H_c.[13]

The recent discovery of $Ni(C_5D_{14}N_2)_2N_3(PF_6)$ NDMAP,[14] a relatively easily crystallized Haldane-gap compound with a critical field of only around 4 T,[15] and no staggering of *g* tensors within spin chains, promises to make the high-field phase readily accessible in neutron scattering studies. The crystal structure of this material is similar to that of NENP, and is visualized in Fig. 1. The antiformagnetic (AF) spin chains run along the *c* axis of the orthorhombic structure (space group P_{nmn}, $a=18.046$ Å, $b=8.705$ Å, and $c=6.139$ Å), and are composed of octahedrally coordinated $S=1$ Ni^{2+} ions bridged by triplets of nitrogen atoms. These long nitrogen bridges account for a relatively small in-chain AF exchange constant $J=2.6$ meV, as estimated from bulk $\chi(T)$ measurements.[15] Specific heat studies revealed a transition to the high-field phase at $H_c^{\parallel}=3.4$ T, and $H_c^{\perp}=5.8$ T, extrapolated to $T\rightarrow0$, for a magnetic field applied parallel and perpendicular to the chain axis, respectively.[15,16] This anisotropy of critical field is attributed to single-ion easy-plane magnetic anisotropy of type DS_z^2. The anisotropy constant was obtained from bulk susceptibility data: $D/J\approx0.3$. Using the well-known numerical result $\Delta_z\approx0.41J+2pD$, $\Delta_x\approx0.41J-pD$, $p\approx2/3$,[6,17] one can thus

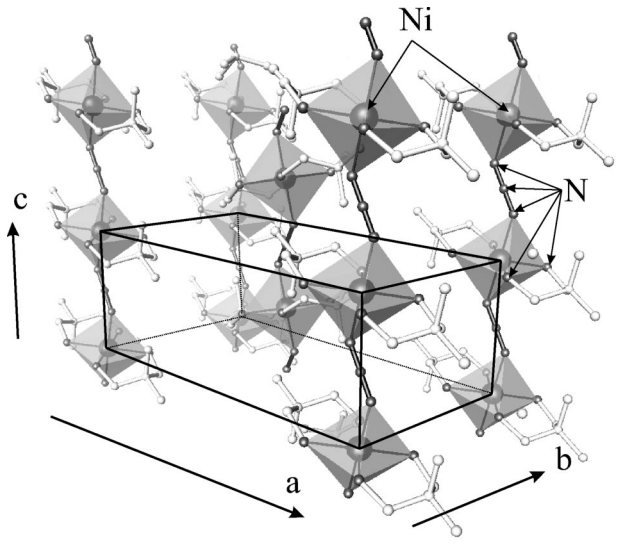

FIG. 1. A schematic view of the antiferromagnetic spin chains in the NDMAP crystal structure. Only Ni, N, and C atoms are shown.

estimate the Haldane gap energies: $\Delta_{\parallel} \approx 2.1$ meV and $\Delta_{\perp} \approx 0.54$ meV.

While NDMAP appears to be an ideal model system for neutron scattering experiments in the high-field phase, additional characterization, particularly a measurement of exchange constants and and anisotropy parameters, is required before such a study can be carried out. Finding the 3D AF zone center is especially important, since it is at this wave vector that static long-range correlations are expected to appear in the high-field phase. In the present paper we report the results of a zero-field inelastic neutron scattering study of deuterated NDMAP single-crystal samples, aimed at obtaining this information.

II. EXPERIMENTAL PROCEDURES AND RESULTS

Fully deuterated NDMAP single-crystal samples were grown from solution as described in Ref. 14. It was observed that the crystals tend to shatter when cooled to low temperature, and even more so when warmed back up. When wrapped in aluminum foil the crystals do not fall apart, but the width of the mosaic distribution increases with thermal cycling. Most inelastic neutron scattering data were collected on a 140 mg single-crystal sample that was taken through the cooling cycle only twice. The mosaic of the as-grown sample was roughly 0.3° and increased to 1.5° and 3° after the first and second cooling, respectively.

High-resolution inelastic neutron scattering measurements were performed on the SPINS three-axis spectrometer installed on the cold neutron source at the National Institute of Standards and Technology Center for Neutron Research (NCNR). Pyrolitic graphite crystals set for their (002) reflection were used as a monochromator and analyzer. Beam divergences were approximately $40' - 80' - 80' - 240'$ through the instrument, with a cooled Be filter between the monochromator and sample. The measurements were done with a fixed final neutron energy $E_f = 2.8$ meV. The crystal

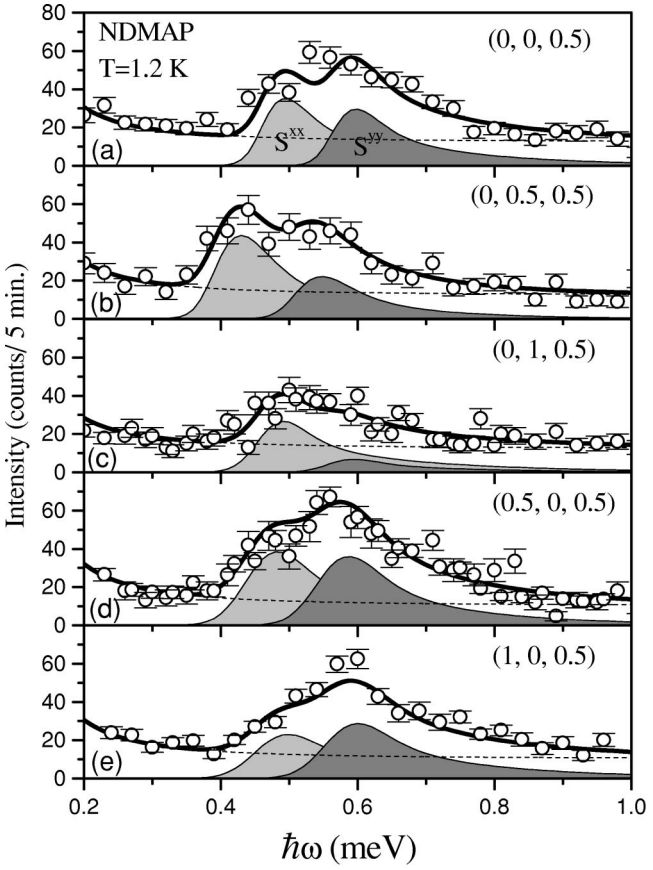

FIG. 2. Typical constant-Q scans measured at $T = 1.2$ K in an NDMAP deuterated single crystal. Solid lines are based on global fits to the data, as described in the text. The shaded areas represent partial contributions of the and b axes polarized Haldane gap excitations to the intensity. The dashed line indicates the background level. The magnetic excitations are resolution limited and peak shapes are entirely defined by resolution effects.

was mounted with either the a or b crystallographic axis vertical, making $(0,k,l)$ and $(h,0,l)$ reciprocal-space planes accessible to measurements. The sample was cooled to $T = 1.4$ K in an ''ILL-Orange'' cryostat with a 70 mm diam sample well.

Most of the data were collected in constant-Q scans at the 1D AF zone center $l = 0.5$ in the energy transfer range $0-1$ meV. In these dispersion measurements wave vector resolution was particularly important, so a flat analyzer was used. Typical scans for different momentum transfers perpendicular to the c axis are shown in Fig. 2. At all wave vectors a well-defined peak corresponding to the lower-energy Haldane excitation doublet is clearly seen around 0.5 meV energy transfer.

To observe the higher-energy Haldane-gap excitation and obtain an accurate measurement of the anisotropy constant we performed a constant-Q scan in the range $0-2.4$ meV (Fig. 3). To maximize intensity we used a horizontally focusing analyzer pointing $\mathbf{c}^*$ towards the analyzer to maintain wave vector resolution along the chain. The scattering angle was varied so the projection of wave vector transfer along the chain was $0.5\mathbf{c}^*$ throughout the scan. In addition to the

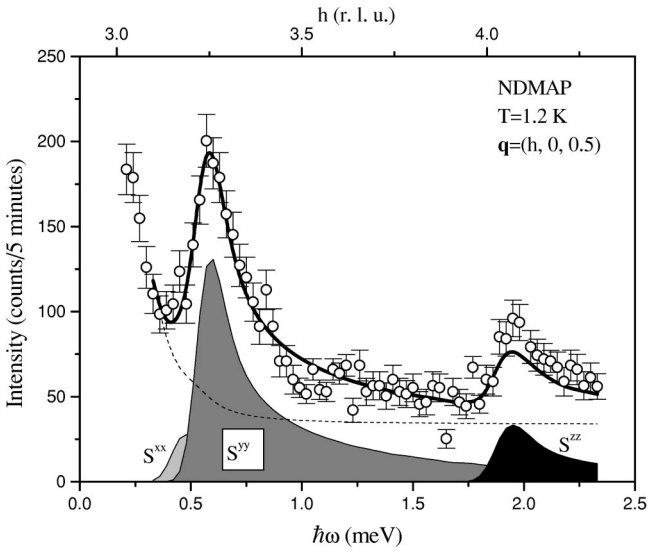

FIG. 3. A constant-$Q_{\parallel}$ scan measured in NDMAP using a horizontally focusing analyzer configuration. Top axis shows the momentum transfer perpendicular to the chain axis. Lines are as in Fig. 2.

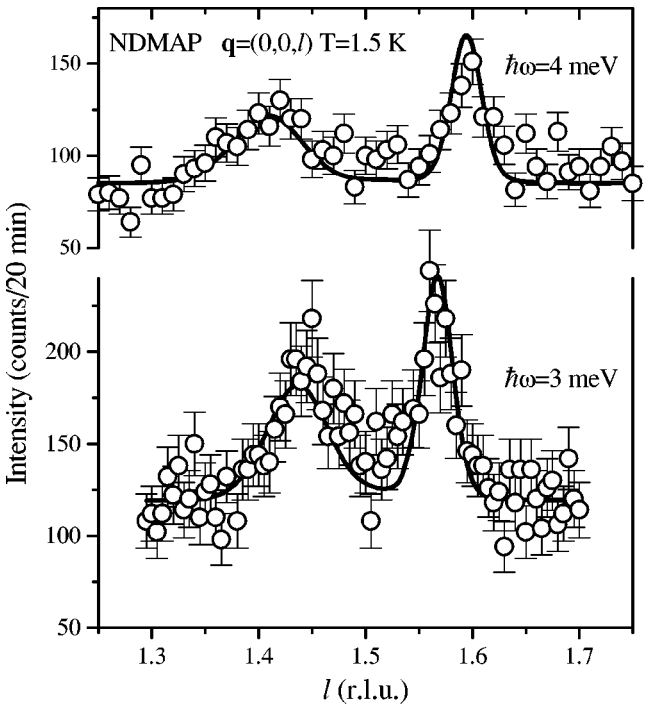

FIG. 4. Constant-energy scans near the 1D AF zone center $l=1.5$ (raw data) , showing the dispersion of Haldane-gap excitations in NDMAP along the chains axis. Solid lines are a fit to the data as described in the text.

peak seen in the low-energy scans, a weaker feature is observed at $\hbar\omega \approx 2$ meV that can be attributed to the *c*-axis-polarized Haldane gap mode.

The steep dispersion along the chains direction is best measured in constant-*E* scans well above the gap energy. Given the small sample size intensity, which for antiferromagnetic spin waves scales as $1/\omega$, becomes a serious limiting factor. To overcome this problem, the measurements were performed in a coarser resolution setup using a thermal neutron beam at the BT-2 three-axis spectrometer at NCNR. 14.7 meV fixed-incident energy neutrons were used with a pyrolitic graphite filter in front of the sample and $60'-60'-60'-\text{open}'$ collimations. Constant-energy scans were collected at 3 and 4 meV energy transfer near the 1D AF zone center $l=1.5$ (Fig. 4). The two spin wave peaks are clearly resolved in both scans. The higher l peak appears sharper then the low l feature due to focusing effects. Note that only transverse excitations contribute to scattering in this geometry.

III. DATA ANALYSIS AND DISCUSSION

The measured constant Q scans were analyzed using a parametrized model cross section, numerically convoluted with the Cooper-Nathans three-axis spectrometer resolution function. Near the 1D AF zone center the single mode approximation (SMA) for the dynamic structure factor of the isolated Haldane spin chain is known to work extremely well.[18,19] For each channel of spin polarization the dynamic structure factor $S^{(\alpha\alpha)}(\boldsymbol{q},\omega)$ can be written as

$$S^{(\alpha\alpha)}(\boldsymbol{q},\omega) \propto |f(q)|^2 \left(1-\frac{\boldsymbol{q}e_\alpha}{q^2}\right)\frac{1-\cos(\boldsymbol{q}c)}{2}\,\frac{Zv}{\omega_{\alpha,\boldsymbol{q}}} \times \delta(\hbar\omega-\hbar\omega_{\alpha,\boldsymbol{q}}), \quad (1)$$

$$(\hbar\omega_{\alpha,\boldsymbol{q}})^2 = \Delta_\alpha^2 + v^2\sin^2(\boldsymbol{q}c). \quad (2)$$

Here v is the spin wave velocity, given by $v \approx 2.49$ J.[20] The dimensionless constant Z defines the static staggered susceptibility of a Haldane spin chain: $\chi_\pi = Zv/\Delta$. (Here we have adopted the notation used in Ref. 22.) In the above expression we have included the magnetic form factor $f(q)$ for Ni^{2+} and the polarization factor $[1-(\boldsymbol{q}e_\alpha/q^2)]$. The structure factor for weakly coupled chains can be calculated in the random phase approximation (RPA).[21] The expression for $S^{(\alpha\alpha)}(\boldsymbol{q},\omega)$ does not change explicitly, but the excitations acquire dispersion perpendicular to the chain axis

$$(\hbar\omega_{\alpha,\boldsymbol{q}})^2 = \Delta_\alpha^2 + v^2\sin^2(\boldsymbol{q}c) + Zv\,J'(\boldsymbol{q}). \quad (3)$$

In this formula $J'(\boldsymbol{q})$ is the Fourier transform of interchain exchange interactions that we assume to be isotropic (of Heisenberg type). According to numerical calculations $Z \approx 1.26$.[20] The form of J' can be guessed by looking at the crystal structure. The smallest interchain Ni-Ni distance (8.705 Å) is along the *b* crystallographic axis. We shall denote the corresponding exchange constant as J_y. The next-smallest interchain Ni-Ni distance (10.478 Å) is along the (0.5,0.5,0.5) direction. This interaction, however, is frustrated by in-chain AF interactions (any site in one chain couples to two consecutive sites in another chain) and is thus irrelevant, within the RPA, at momentum transfers $\boldsymbol{q}c \approx \pi$. Finally, the third smallest interchain distance (18.046 Å) is along *a*. The corresponding coupling constant J_x is expected

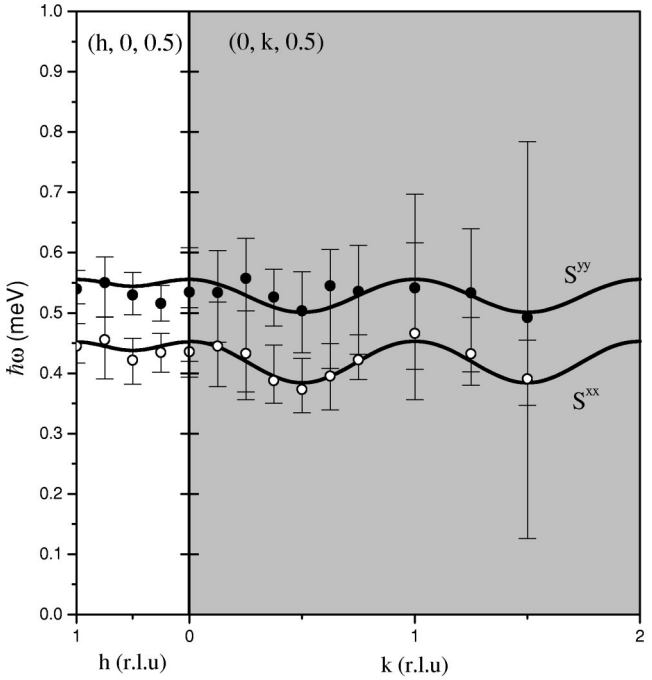

FIG. 5. Transverse dispersion of lower-energy Haldane-gap excitations in NDMAP, determined in global fits to constant-Q scans (solid lines), as described in the text. The data points represent excitation energies obtained in fits to individual scans.

to be very small, due to the large ''bond'' length. The Fourier transform of interchain interactions can thus be written as

$$J'(\boldsymbol{q}) = 2J_x\cos(\boldsymbol{q}a) + 2J_y\cos(\boldsymbol{q}b). \tag{4}$$

The relevant parameters of the model are thus the three gap energies Δ_x, Δ_y, and Δ_z, three exchange parameter J, J_x, and J_y, and an overall intensity prefactor. For constant Q scans three additional parameters were used to describe the background: an energy-independent component, and the intensity and width for a Lorenzian profile centered at $\hbar\omega = 0$ to account for incompletely resolved elastic scattering. The background was assumed to be flat in the constant-E scans measured in the thermal-neutron setup.

The difference between Δ_x and Δ_y, usually a result of in-plane magnetic anisotropy of type $E(S_x^2 - S_y^2)$, is too small to yield resolved peaks with the resolution of our instrument. Distinct polarization factors for the two branches, however, allow us to extract both parameters in a global fit to the data measured at different momentum transfers perpendicular to the chain axis. As a first step, we simultaneously analyzed the data collected in $(0,k,l)$ reciprocal-space plane (11 scans with a total of 382 data points). A very good global fit using Eqs. (1) and (3) is derived with a residual $\chi^2 = 1.6$. The solid lines in Figs. 2(a)–2(c) were calculated from the globally optimized parameter set. The shaded areas represent the contribution of each mode, and the dashed lines show the background level. Figure 5 (right) shows the obtained b-axis dispersion relation (solid line), that has a minimum at $k = 0.5$. Symbols in this figure represent the excitation energies obtained in fits to individual scans. A similar global fit (four scans, 149 data points, $\chi^2 = 1.7$) was applied to all constant Q scans measured in the $(h,0,l)$ scattering plane [solid lines in Figs. 2(d) and 2(e)]. In this case the excitation energies at the zone boundary (0,0,0.5) were fixed to the values obtained from the $(0,k,l)$ plane global fit. Only the a-axis exchange constant J_x was refined. Dispersion of magnetic excitations along this direction is barely detectable, $J_x = 0$ being within the experimental error bar. The resulting dispersion relation is nontheless plotted in a solid line in Fig. 5 (left). The final values of parameters determined in the least-squares analysis are as follows: $\Delta_x = 0.42(3)$ meV, $\Delta_y = 0.52(6)$ meV, $J_y = 1.9(1)\times 10^{-3}$ meV, and $J_x = 4(3)\times 10^{-4}$ meV. from the inelastic measurements we can only conclude that the global minimum of the 3D dispersion (3D AF zone center) is located somewhere on the $(h,0.5,0.5)$ reciprocal-space rod.

To verify that the splitting of the excitation doublet is indeed a relevant parameter, we have also analyzed the measured constant-Q scans assuming $\Delta_x \equiv \Delta_y$. To obtain good fits to individual scans using this model, we were forced to allow the magnetic excitations to have a nonzero intrinsic energy width. However, even including this additional parameter did not allow us to get a good agreement in a global fit to all measured constant-Q scans. The excitation energy determined from fits to scans collected in the $(0,k,l)$ plane at large values of momentum transfer perpendicular to the chain axis were found to be consistently smaller than at equivalent reciprocal-space points at smaller k. This behavior is consistent with having two separate resolution-limited modes at slightly different energies, the intensity of the higher-energy mode being suppressed by the polarization factor at large k, but not with the $\Delta_x \equiv \Delta_y$ model.

The energy gap for c-axis polarized excitations was determined by fitting the model cross section to the wide-range constant-Q scan measured with the horizontally focusing configuration (Fig. 3, solid line). In this procedure the values of Δ_x and Δ_y were fixed. The analysis yields $\Delta_z = 1.86(0.1)$ meV.

The in-chain exchange constant was determined by fitting the SMA cross section to the measured constant-E scans. The gap energies were fixed at the values quoted above and only J, a flat background, and an intensity factor were refined to best fit the data (solid line in Fig. 4). The obtained value $J = 2.8(1)$ meV is in good agreement with the result of Ref. 15. The anisotropy constant D is straightforward to estimate from the measured gap energies:[6,17] $D \approx \frac{1}{4}(2\Delta_z - \Delta_x - \Delta_y) = 0.70$ meV, and $D/J = 0.25$, which is also consistent with the bulk susceptibility result of Ref. 15. The relative strength of interchain interactions are $J_y/J \approx 6\times 10^{-4}$ and $J_x/J < 1.0\times 10^{-4}$. These ratios are very similar to those found in NENP.[3]

We would like to note that while the gap energies and the spin wave velocity measured with inelastic neutron scattering in this work are in excellent agreement with the results of susceptibility and high-field magnetization and specific heat studies,[15] there appears to be a discrepancy with ESR results of Ref. 16. Weak ESR absorbtion lines in NDMAP occur at 0.05, 0.4 and 0.48 meV, extrapolated to zero field. For a uniform-chain Haldane antiferromagnet, low-energy ESR

lines are associated with transitions between components of the Haldane triplet that become thermally populated at nonzero temperature. The energy of the 0.05 meV ESR line is consistent with it being a transition between the lower-energy doublet of transverse excitations ($\Delta_y - \Delta_x = 0.10(7)$ meV, according to our neutron data). However, the other two resonance energies are much smaller than the doublet-singlet splitting observed in this work. The resonances are instead close to the values of the transverse Haldane gap energies themselves. Coupling to the $q = \pi$ Haldane mode by electron spin resonance (ESR) may in fact occur due to impurity effects. Further studies will be required to fully understand the ESR spectra.

IV. SUMMARY

The lowest-energy excitation in NDMAP is polarized along the crystallograhic *a* axis. The 3D magnetic zone center is located on the $(h,0.5,0.5)$ reciprocal-space rod. Future experimental studies of the high-field phase should thus concentrate on this region of reciprocal space.

ACKNOWLEDGMENTS

We would like to thank S. M. Shapiro for illuminating discussions, S.-H. Lee for his assistance with the measurements at NIST, and R. Rothe for technical support at Brookhaven National Laboratory (BNL). Work at was carried out under Contract No. DE-AC02-98CH10886, Division of Material Science, U.S. Department of Energy. Work at Johns Hopking University (JHU) was supported by the NSF through Grant No. DMR-9801742. This work used instrumentation supported by NIST and the NSF through DMR-9423101. Work at RIKEN was supported in part by a Grant-in-Aid for Scientific Research from the Japanese Ministry of Education, Science, Sports and Culture.

[1] F.D.M. Haldane, Phys. Lett. **93A**, 464 (1983); Phys. Rev. Lett. **50**, 1153 (1983).

[2] For a comprehensive list of references, see, for example, M. Enderle *et al.*, Europhys. Lett. **25**, 717 (1994); I.A. Zaliznyak, L.-P. Regnault, and D. Petitgrand, Phys. Rev. B **50**, 15824 (1994).

[3] See reference list in L.P. Regnault, I. Zaliznyak, J.P. Renard, and C. Vettier, Phys. Rev. B **50**, 9174 (1994).

[4] J. Darriet and L.P. Regnault, Solid State Commun. **86**, 409 (1993); J.F. DiTusa *et al.*, Physica B **194–196**, 181 (1994); T. Yokoo, T. Sakaguchi, K. Kakurai, and J. Akimitsu, J. Phys. Soc. Jpn. **64**, 3651 (1995); G. Xu *et al.*, Phys. Rev. B **54**, R6827 (1996).

[5] L.P. Regnault, C. Vettier, J. Rossat-Mignod, and J.P. Renard, Physica B **180–181**, 188 (1992).

[6] O. Golinelli, T. Jolicoeur, and R. Lacaze, J. Phys.: Condens. Matter **5**, 7847 (1993).

[7] K. Katsumata *et al.*, Phys. Rev. Lett. **63**, 86 (1989).

[8] I. Affleck, Phys. Rev. B **41**, 6697 (1990).

[9] T. Sakai and M. Takahashi, J. Phys. Soc. Jpn. **62**, 750 (1993).

[10] M. Chiba *et al.*, Phys. Rev. B **44**, 2838 (1991).

[11] P.P. Mitra and B.I. Halperin, Phys. Rev. Lett. **72**, 912 (1994).

[12] T. Sakai and H. Shiba, J. Phys. Soc. Jpn. **63**, 867 (1994).

[13] M. Enderle, L.-P. Regnault, C. Broholm, D. H. Reich, I. Zaliznyak, M. Sieling, and B. Lüthi (unpublished)

[14] M. Monfort, J. Ribas, X. Solans, and M. Font-Bardia, Inorg. Chem. **35**, 7633 (1996).

[15] Z. Honda, H. Asakawa, and K. Katsumata, Phys. Rev. Lett. **81**, 2566 (1998).

[16] Z. Honda, K. Katsumata, M. Hagiwara, and M. Tokunaga, Phys. Rev. B **60**, 9272 (1999).

[17] S.V. Meshkov, Phys. Rev. B **48**, 6167 (1993).

[18] S. Ma *et al.*, Phys. Rev. Lett. **69**, 3571 (992).

[19] G. Xu *et al.*, Phys. Rev. B **54**, R6827 (1996).

[20] E.S. Sorensen and I Affleck, Phys. Rev. B **49**, 15771 (1994).

[21] R.M. Morra, W.J.L. Buyers, R.L. Armstrong, and K. Hirakawa, Phys. Rev. B **38**, 543 (1988).

[22] S. Maslov and A. Zheludev, Phys. Rev. Lett. **80**, 5786 (1998).